Na-23 NMR Spectroscopic Quantification of the Antiferroelectric-Ferroelectric Phase Coexistence in Sodium Niobate

Egert, Sonja; Zhang, Mao-Hua; Koruza, Jurij; Groszewicz, Pedro B.; Buntkowsky, Gerd

DOI
10.1021/acs.jpcc.0c07202

Publication date
2020

Document Version
Final published version

Published in
Journal of Physical Chemistry C

THE JOURNAL OF PHYSICAL CHEMISTRY C

pubs.acs.org/JPCC Article

^{23}Na NMR Spectroscopic Quantification of the Antiferroelectric–Ferroelectric Phase Coexistence in Sodium Niobate

Published as part of The Journal of Physical Chemistry virtual special issue "Hellmut Eckert Festschrift".

Sonja Egert, Mao-Hua Zhang, Jurij Koruza, Pedro B. Groszewicz,* and Gerd Buntkowsky*

Cite This: *J. Phys. Chem. C* 2020, 124, 23852–23858 Read Online

ABSTRACT: The irreversible field-induced phase transition between the antiferroelectric (*P*) and ferroelectric (*Q*) polymorphs of sodium niobate ($NaNbO_3$) ceramics constitutes a focal point in improving the material's energy storage properties. The coexistence of *P* and *Q* phases can be verified by X-ray and electron diffraction methods, but its extent remains elusive. Two-dimensional solid-state nuclear magnetic resonance (NMR) spectroscopy allows the quantification of relative amounts of the coexisting polymorphs, but the analysis of ceramic sample pieces requires a trade-off between sufficient sensitivity (at higher magnetic fields) and separation of the overlapping *P* and *Q* signals (at lower magnetic fields). In this contribution, we apply the satellite transition magic angle spinning (STMAS) pulse sequence in a quantitative analysis of the antiferroelectric–ferroelectric phase transition in $NaNbO_3$ ceramics. Both field- and grain size-induced transitions are investigated and the coexistence of the *Q* and *P* phases after the application of an electric field is quantified to be approximately 50%:50%. No indication is found that the local structure of the field-induced *Q* polymorph differs fundamentally from that induced in small-sized grains. Furthermore, the sensitivity and resolution of STMAS is compared to previously reported applications of the triple quantum magic angle spinning (3QMAS) sequence to the $NaNbO_3$ system.

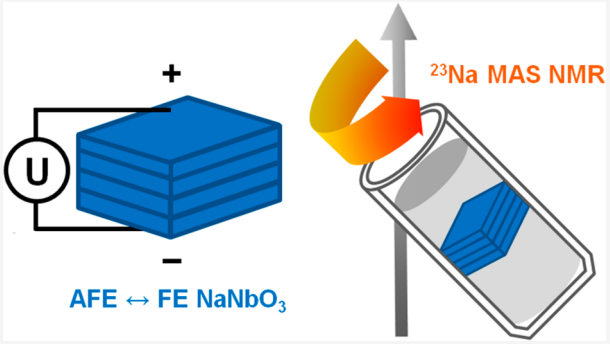

INTRODUCTION

As antiferroelectrics constitute a promising class of high-performance functional materials in energy storage applications, interest arises to replace lead-based materials with more environmentally friendly lead-free ones.[1,2] This requires a thorough understanding of the relationship between the atomic structure and resulting properties. Special attention should be paid to the structural changes accompanying the antiferroelectric–ferroelectric (AFE–FE) phase transition, which is crucial for energy storage applications.

Promising lead-free antiferroelectrics are derived from sodium niobate ($NaNbO_3$), the phase stability of which can be tailored by compositional modification.[3] One of the main goals of developing new, lead-free $NaNbO_3$-based solid solutions is to find appropriate modifications that will make the AFE–FE transition reversible at room temperature and thus enable the design of capacitors with a high energy density.[3−5] To this end, a thorough understanding of the structural origins of this transition is crucial, and it is necessary to have a tool at hand that enables us to monitor the degree of reversibility. The quantification of phase coexistences before and after the application of an electric field contributes to that aim and, in consequence, enhances our understanding of the material properties.

In pure $NaNbO_3$, the AFE–FE transition is accompanied by a structural transition from the room-temperature *P* polymorph (space group No. 57, *Pbma*) to the *Q* polymorph (No. 26, $Pmc2_1$).[6,7] The transition can either be induced by an electric field[8−10] or by reducing the grain size to the submicrometer range.[11] The two structures are closely related—indeed, $Pmc2_1$ is a subgroup of *Pbma*—and merely exhibit subtle changes in the octahedral tilt system of the perovskite structure. In diffraction methods, only the low-intensity superlattice reflections are affected by these differences[12] and in consequence, they are difficult to track, let alone quantify. The matter is further complicated by the frequently occurring coexistence of both phases in single crystals[13,14] and ceramics.[10,15] Additionally, the phase composition is sensitive to the employed synthesis strategy.[16,17]

Received: August 6, 2020
Revised: September 29, 2020
Published: September 29, 2020

https://dx.doi.org/10.1021/acs.jpcc.0c07202
J. Phys. Chem. C 2020, 124, 23852–23858

Solid-state nuclear magnetic resonance (NMR) spectroscopy reveals the structure of materials on a local scale, reflecting, among others, the coordination, symmetry, and bond distances of the probed nuclei.[18] Even in highly disordered materials featuring a broad distribution of structural parameters, two-dimensional NMR methods can be utilized to reveal and analyze coexisting species.[19] As Johnston et al. have highlighted in their previous study of $NaNbO_3$, NMR spectroscopy is well-suited to monitor local structural changes occurring in the cation environments and, in extension, changes to the octahedral tilt system and related phase transitions.[12]

^{23}Na ($I = {}^3/_2$) is a fairly sensitive NMR nucleus due to its high natural abundance and gyromagnetic ratio. The challenge in recording ^{23}Na NMR spectra lies in the quadrupolar broadened lines and the relatively small chemical shift dispersion,[17] resulting—in the case of $NaNbO_3$—in overlapping lines (Figure 1). While the signals of the two

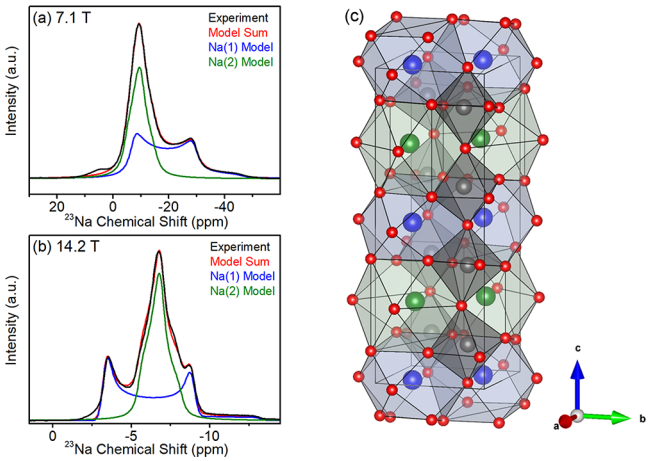

Figure 1. Deconvolution of ^{23}Na NMR spectra of *P* $NaNbO_3$ recorded at (a) 7.1 T and (b) 14.2 T with two lines corresponding to the two sodium sites Na(1) and Na(2). The Na(1) line shape reflects an asymmetry parameter $\eta = 0$, whereas for Na(2) $\eta \approx 1$. If the *P* and *Q* polymorphs coexist in a sample, an additional line with $\eta \approx 1$ corresponding to the *Q* Na(1) site overlaps with the other two, rendering the deconvolution unreliable. While at 14.2 T the one-dimensional spectrum is more clearly defined, at 7.1 T the overlapping *P* and *Q* Na(1) signals can be separated in the indirect dimension using the 3QMAS or STMAS sequence. (c) Unit cell of the $NaNbO_3$ *P* polymorph with two sodium sites (Na(1), blue and Na(2), green). Image made using the VESTA software.[20]

inequivalent sodium sites Na(1) and Na(2) present in its structure cannot be resolved in one-dimensional NMR spectra, NMR is still sensitive to the differences (local symmetry, isotropic chemical shift, and strength of quadrupolar coupling) between the Na(1) and Na(2) sites as well as between the *P* and *Q* polymorphs, and two-dimensional NMR methods can be employed to distinguish between them.

Previous publications[11,12,17] have demonstrated the triple-quantum magic angle spinning (3QMAS) NMR sequence to be capable of distinguishing between *P*- and *Q*-$NaNbO_3$. The dramatic change of the Na(1) NMR line shape due to the change of local symmetry allows for an unambiguous assignment of the Na(1) signals of both polymorphs. Even though 3QMAS is not strictly a quantitative method, it has been noted that the relative intensities of signals with similar quadrupolar coupling constants, such as the Na(1) signals of the *P* and *Q* phase, can be interpreted in a quantitative way.[12]

In the aforementioned publications, two different methods of quantifying the coexistence of *P* and *Q* phases were established. As Figure 1 illustrates, the line shape of $NaNbO_3$ NMR spectra varies with the magnetic field strength, reflecting the dependence of the chemical shift and quadrupolar interactions on it. The interplay of the two interactions determines the position of the signal in 3QMAS spectra. At low magnetic fields, the Na(1) signals of the *P* and *Q* phase can be separated in the indirect dimension of the 3QMAS spectrum, and relative intensities can thus directly be evaluated. At higher magnetic fields, *P* and *Q* signals will partially or completely overlap, but can still be separated by a line shape deconvolution similar to the ones shown in Figure 1.[11] It should be noted that, in the latter method, an assumption on the structural model has to be made and that the line shapes obtained may be distorted due to nonuniform excitation and conversion of the triple-quantum coherences.[12]

In order to study the field-induced transition in $NaNbO_3$ and similar ceramics with NMR, a ceramic piece on which electrodes can be applied is required. The high fields necessary to induce this phase transition[10] and the limited electric field strengths achievable in laboratory devices severely limit the thickness of samples, whereas standard NMR rotor sizes are the restrictive factor for the other two dimensions of the sample. From a practical point of view, this means that the experimentalist will have to work with small sample sizes (typically ca. 10−30 mm^3). Such a small sample amount can be problematic for a 3QMAS experiment due to the low sensitivity rooted in the poor efficiency of triple-quantum excitations. This difficulty is amplified by the dependence of excitation efficiency on the quadrupolar coupling constant, resulting, in the case of $NaNbO_3$, in a less efficient excitation of the Na(1) signals of interest. On top of this, working at low magnetic fields in order to separate the *P* and *Q* signals directly comes at the additional cost of an inherently lower signal-to-noise ratio.

In turn, Ashbrook et al. have suggested that the satellite transition magic angle spinning (STMAS) sequence might find application in the study of small sample amounts.[21] While slightly more elaborate to set up and more sensitive to magic angle misalignments as well as MAS rate instabilities, STMAS has been shown to be generally superior in terms of sensitivity.[21,22] The different contributions to line broadening that can occur in STMAS spectra make it difficult to pass an absolute verdict on the two methods with respect to their spectral resolution, thus motivating comparisons of the methods for specific material systems.[22,23] STMAS spectra can be interpreted in a quantitative way within the same limitations as 3QMAS spectra, and have been noted by Ashbrook et al. to even be "less nonquantitative" in general.[21]

In this work, we demonstrate how the analysis of the phases related to the AFE−FE transition in $NaNbO_3$ can benefit from the enhanced sensitivity of STMAS. STMAS allows for the acquisition of NMR spectra at a relatively low magnetic field of 7.1 T while maintaining reasonable experimental times and signal-to-noise ratio even for sample amounts in the range of a few cubic millimeters. Recently, we employed this technique in a study of the irreversible transition observed in $NaNbO_3$ ceramics to quantify the coexistence of AFE and FE phases.[10] Here, we aim to give a deeper insight into the evaluation of the available methods. Additionally, we compare $NaNbO_3$ with different grain sizes to exemplarily analyze the trade-off between STMAS and 3QMAS when working at a lower

https://dx.doi.org/10.1021/acs.jpcc.0c07202
J. Phys. Chem. C 2020, 124, 23852−23858

magnetic field (for a more detailed explanation of both methods see refs 21, 22, and 24). It is demonstrated that relative amounts of *P* and *Q* phases can be determined even in samples where they have previously not been accessible, and local structural evidence for the coexistence of the polymorphs in both cases is brought forward. Our goal is to provide analysis of available ^{23}Na NMR methods for the investigation of $NaNbO_3$–based antiferroelectrics, laying a basis for the improved understanding of AFE–FE phase transition.

METHODS

$NaNbO_3$ samples were prepared by a solid-state reaction from Na_2CO_3 (99.95%, Alfa Aesar, Germany) and Nb_2O_5 (99.90%, Alfa Aesar, Germany) as previously described.[10] To induce the AFE–FE phase transition in the $NaNbO_3$ samples, six pieces (2.3 × 2.3 × 0.4 mm^3) were cut out of ceramic discs and subjected to an electric field of 12 kV/mm at room temperature. All samples exhibited a longitudinal piezoelectric coefficient d_{33} of zero before application of the electric field and 35 ± 1 pC/N afterward, reflecting the presence of macroscopic piezoelectricity. Six pellets were stacked on top of each other and fitted into the center of a 4 mm zirconia MAS rotor. The high electric fields required to effectively induce the FE phase in $NaNbO_3$ dictate a thickness of 0.4 mm for each piece and whereas it is possible to record an NMR signal with an amount of sample this low, the stacking allows for a better signal-to-noise ratio. Within the set of samples with different grain sizes, single ceramic pieces with dimensions of 4.8 × 2.7 × 1.2 mm^3 (average grain size of 0.19 μm) and 5.4 × 2.9 × 1.7 mm^3 (1.07 μm) were used. The free space of the rotor was filled up with TiO_2 powder to allow for stable magic angle spinning at 10000 ± 1 Hz. ^{23}Na STMAS experiments were performed on a *Bruker Avance III* spectrometer operating at a magnetic field of 7.1 T. A double-quantum and *z*-filtered sequence was employed, and 110 increments were acquired averaging 2128 transients with a relaxation delay of 1 s. The excitation and mixing pulses were 1.4 and 2.1 μs, respectively, whereas selective 90 and 180 deg pulses were 21.75 and 40.75 μs. The ^{23}Na chemical shift was referenced to the signal of $NaNO_3$(s) at −8.1 ± 0.1 ppm.[25] The magic angle was set with care using the ^{87}Rb STMAS spectrum of $RbNO_3$ and the angle stability with respect to the rotor ejection and insertion under gas flow was confirmed. For ^{23}Na 3QMAS experiments, a *z*-filtered sequence with 110 increments averaging 2136 transients was used. The relaxation delay was set to 1 s and excitation, mixing, and selective 90 deg pulses were 6.17 μs, 1.8 μs, and 17 μs, respectively. NMR parameters were determined by line shape simulations using DMFit.[26] Commercial $NaNbO_3$ was purchased from Alfa Aesar (99.997%).

RESULTS AND DISCUSSION

From a local structural viewpoint, the most drastic change occurring during the AFE–FE transition in $NaNbO_3$ is the loss of the axial, or 4-fold rotational, symmetry of the sodium Na(1) site within the NaO_{12} cuboctahedron. The relative arrangement of the oxygen atoms around the sodium site is mainly responsible for the size and symmetry of the electric field gradient (EFG) tensor, the asymmetry parameter (η) of which changes from $\eta = 0$ to $\eta \approx 1$ for this specific phase transition, indicating the loss of axial symmetry in the structure.

Before subjecting the samples to an electric field, the ^{23}Na STMAS spectrum of six stacked $NaNbO_3$ pieces depicted in Figure 2a was recorded. In the two-dimensional spectrum, the

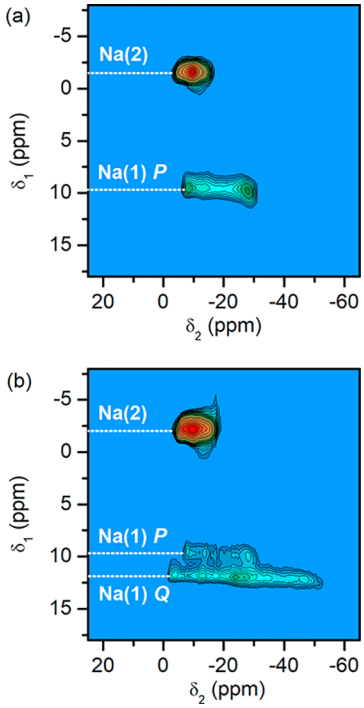

Figure 2. ^{23}Na STMAS spectra of ceramic $NaNbO_3$ before (a) and after (b) subjecting the samples to an electric field to induce the AFE–FE phase transition. At a magnetic field of 7.1 T, the signals corresponding to the *P* (η =0) and *Q* ($\eta \approx 1$) polymorphs of sodium site Na(1), respectively, can be separated in the indirect dimension δ_2. This allows for a quantification of the two phases by integration along the indirect axis.

signals of sodium sites Na(1) and Na(2) are separated in the indirect dimension (δ_1). Only these two signals are visible and both the position (δ_1 = 9.5 ppm) and the presence of two maxima (asymmetry parameter η = 0) for the lower signal are indicative of the Na(1) site in the *P* polymorph. As subjecting the samples to an electric field results in a significant change of the d_{33} parameter from 0 to 35 ± 1 pC/N indicating the presence of macroscopic piezoelectricity, it is expected that a signal corresponding to the *Q* phase will be present in the corresponding STMAS spectrum. In order to avoid overlapping of *Q* and *P* phase signals, a low magnetic field of 7.1 T is chosen deliberately based on the respective field-dependency of the chemical shift and second-order quadrupolar interaction.[17] Indeed, the spectrum in Figure 2b exhibits an additional signal at δ_1 = 12.1 ppm with a single maximum (i.e., asymmetry parameter $\eta \approx 1$) that can be attributed to the *Q* polymorph. While an even lower magnetic field would provide higher resolution between signals with similar quadrupolar coupling constants, as the Na(1) in *P* and *Q* phases, this choice would be detrimental to the signal-to-noise ratio and perhaps impair the quantitative aspects of the method. For a comparison with an STMAS spectrum at higher magnetic field refer to the Supporting Information, Figure S1.

While the two signals are not completely separated, they are resolved enough to quantify their relative amounts. This is apparent when considering the sum of the signals projected on the indirect axis (Figure 3). The profile of the Na(1) *P* signal

https://dx.doi.org/10.1021/acs.jpcc.0c07202
J. Phys. Chem. C 2020, 124, 23852−23858

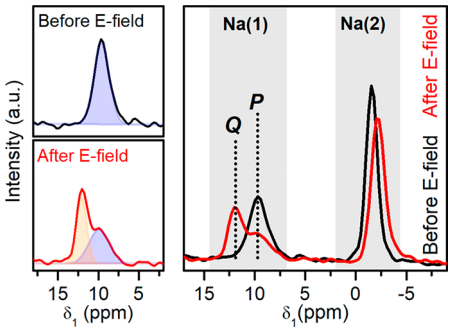

Figure 3. Projections along the indirect axes of the ^{23}Na STMAS spectra displayed in Figure 2. The separation of the signals is sufficient to allow for the extraction of the quantity of *P* and *Q* polymorph in the sample according to the procedure explained in the text. The relative amounts of the coexisting phases are determined to be 50 ± 5% *P* and 50 ± 5% *Q* after the field-induced phase transition.

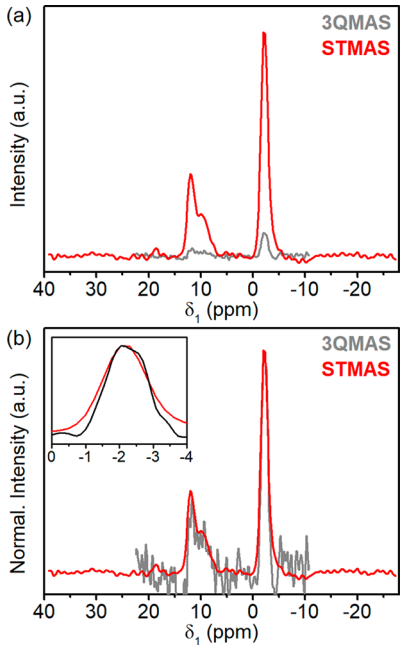

Figure 4. Projections along the indirect axes of ^{23}Na STMAS (red) and 3QMAS (gray) experiments of stacked $NaNbO_3$ pellets after subjection to an electrical field, (a) not normalized and (b) normalized. Totals of 2128 and 2136 transients were averaged, respectively, for each of the 128 increments, and relaxation times were 1 s. The sensitivity gain of STMAS over 3QMAS determined from the integrals of the Na(2) signal is approximately 11:1. An expected small splitting between the Na(2) signals of the *P* and *Q* polymorphs is observed in the 3QMAS spectrum, but not in the STMAS spectrum, indicating the slightly higher resolution achieved with the 3QMAS sequence.

at δ_1 = 9.7 ppm in untreated $NaNbO_3$ is a symmetric Gaussian, indicating pure *P* polymorph. In turn, after subjecting the sample to an electrical field *ex situ*, the *Q* signal appears at δ_1 = 11.9 ppm, with the *P* signal remaining as a shoulder to the *Q* signal. From a deconvolution of the lines with two Gaussian functions, the relative amounts of the coexisting phases are determined as 50 ± 5% *P* and 50 ± 5% *Q* after electric field application.[10]

The performance of STMAS can be compared to 3QMAS with respect to both the signal intensity (reflecting the excitation efficiency) and the signal width (reflecting the resolution). Figure 4 displays projections on the indirect dimension (δ_1) from spectra recorded for the same stack of samples for each method using a similar number of scans and the same relaxation delay and number of increments. It is obvious from Figure 4a that the sensitivity gain is significant (signal area increase of approximately ×11) whereas Figure 4b shows that the line widths remain comparable for normalized intensities. Despite the lower sensitivity, an argument can be made for the higher resolution of the 3QMAS spectrum. A small chemical shift difference of 0.7−0.9 ppm is expected between the Na(2) sites of the *P* and *Q* phases.[12] While such a splitting is observed in the 3QMAS spectrum as the presence of two maxima for the Na(2) signal (inset in Figure 4b), the STMAS spectrum only exhibits a singular broadened signal for this sodium site. Still, we consider the slight difference in resolution nonsignificant compared to the sensitivity gain and the resulting sufficient signal-to-noise ratio of the Na(1) signal allowing for fitting and quantification in the first place. Several possible explanations of the enhanced sensitivity of STMAS have been suggested in the literature, noting that typical enhancement factors range in the order of 4−5.[21] On the other hand it should also be noted that STMAS spectra tend to exhibit more "t1 noise",[21] often necessitating a baseline correction before quantification and contributing to the error interval of ±5% estimated for the quantification of relative amounts of *P* and *Q* phases.

Since no difference can be observed for the signal widths of the ceramic samples, we also compared the resolution and sensitivity of commercially purchased $NaNbO_3$ powder (predominantly *P*-phase) in order to obtain a more complete picture. Here, it was found that the width of the Na(2) line increased approximately by a factor of 1.6 from 3QMAS to STMAS (see Figure S2), which can be considered a significant disadvantage. We consider the most probable explanation to be the larger influence of slight magic angle misalignments and MAS rate instabilities on STMAS line widths.[22,23] Moreover, we observe that 3QMAS spectra of the pellet samples appear broader as the line-width of the powder samples (Na(2) line width is 1.41 ppm for the pellet, but only 0.65 ppm for the powder), which may be attributed to a lower crystallinity of the pellet samples.[17] The sensitivity gain of STMAS over 3QMAS for powdered samples was only observed to be approximately 3.6:1. It is possible that this difference can be accounted for by inhomogeneities of the RF coil: While the ceramic sample measured only 2.4 mm in height and was placed exactly in the center of the rotor, for the powder measurements the middle third of the rotor was filled completely.

One should note that the stacking of several ceramic pieces after subjecting them to an electric field may have an influence on the structural information that can be obtained from the STMAS spectra, besides the increase of the signal-to-noise ratio. Parameters related to the local environment of the sodium ions can be obtained from projections along the direct dimension, resulting in pseudo-1D spectra of the isolated sodium sites (dashed lines in Figure 2b). Figure 5 displays lines corresponding to the Na(1) sites in the *P* and *Q* polymorph of the samples after application of the electric field. As expected, the *P* signal exhibits two maxima (corresponding to an asymmetry parameter η = 0) and a quadrupolar coupling constant of $C_Q \approx 2.1$ MHz. From the width and shape of the *Q* signal, $\eta \approx 1$ and $C_Q \approx 2.1$ MHz can be deduced, again matching the expectations. However, while the qualitative line

https://dx.doi.org/10.1021/acs.jpcc.0c07202
J. Phys. Chem. C 2020, 124, 23852−23858

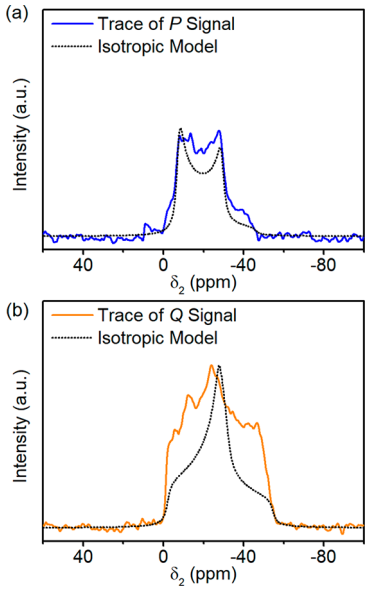

Figure 5. Projections along the direct dimension of the ^{23}Na STMAS Na(1) signals in six stacked $NaNbO_3$ pellets after the subjection to the electrical field: (a) *P* polymorph and (b) *Q* polymorph. As a guide for the eye, simulations of isotropic lines with C_Q = 2.13 MHz have been added, illustrating the mismatch of the relative intensities of maximum and signal body in the case of the *Q* polymorph.

shape with two sharp singularities and a single maximum fits with the expected local structure, the relative intensity of the maximum compared to the body of the line does not.

In a polycrystalline sample, the line shape produced by the second order quadrupolar interaction and observed here depends on the size and direction of the electric field gradient tensor and, as a result, on grain or domain orientation. Therefore, a possible explanation for this observation can be the prevalence of a nonisotropic distribution of the grains or domains which have undergone the *P*−*Q* transition, thus indicating that some sort of preferential orientation of local structural environments occurs along the polarization axis in the course of the ferroelectric ordering. It must also be considered that it could be merely an effect of nonuniform excitation. However, the projections obtained for the samples with different grain sizes (which consist of a single piece of isotropic ceramics and have not been subjected to an electrical field) shown in the supplementary data in Figure S3 do not exhibit the same deviation from the expected isotropic line shape, which would be expected for a systematically nonuniform excitation. Within the context of quantification of coexisting polymorphs in $NaNbO_3$, the observed effect illustrates that the assumptions made on line shapes in polycrystalline samples are not always reflected experimentally, thus further complicating the attempt of quantification by line shape fitting.

While the ferroelectric *Q* phase in $NaNbO_3$ is mainly known as the electric-field induced room temperature phase, it has previously been shown that this phase transition is also induced when grain sizes of polycrystalline $NaNbO_3$ are reduced below 0.27 μm.[11] Additionally, coexistence of the *P* and *Q* polymorphs occurs for ceramic samples which exhibit a wide range of grain sizes with their ratios changing as a function of the grain size distribution.[11] In a previous publication, this phase coexistence was analyzed using 3QMAS at a higher magnetic field of 14.2 T, and by fitting the extracted Na(1) signal projection along the direct dimension—at this field strength, an overlap of *P* and *Q* signals—with two lines corresponding to $\eta = 0$ and $\eta \approx 1$.[11] The main difficulty of this procedure is the distortion of the projections due to nonuniform excitation of triple-quantum coherences. While the high sensitivity of STMAS allows for the acquisition of spectra at lower magnetic field within reasonable experimental time and the resolution of *P* and *Q* signals in the indirect dimension, the argument can be made that the experimental expense of setting up the STMAS pulse sequence is not worth the trade-off. Therefore, to account for a more complete picture of the method comparison as well as the nature of the *P*−*Q* transition in $NaNbO_3$, we recorded STMAS spectra at 7.1 T of two samples of different grain sizes. A sample with an average grain size of 1.07 μm was expected to be pure *P* polymorph within the error interval of the previous investigation, whereas for the sample with an average grain size of 0.19 μm, 85% *Q* polymorph had been reported.[11]

In the STMAS spectrum for the large-grain sample in Figure 6a, the presence of the *Q* polymorph signal around 12 ppm in the indirect dimension is not obvious and, in fact, merely recognizable as an asymmetry of the Na(1) signal. The indirect projection depicted in Figure 6b, however, reveals a broad shoulder indicating that a considerable portion of the *Q* polymorph is still present.

It should be noted that the relatively low quantity of the *Q* phase results in the signals being less well resolved, and we assume the accuracy of quantification to be lower. However, a still significant amount of 20% *Q* polymorph is estimated. For the sample with the smaller grain size (analogous analysis in Figure 6, parts c and d), in turn 75% *Q* polymorph can be

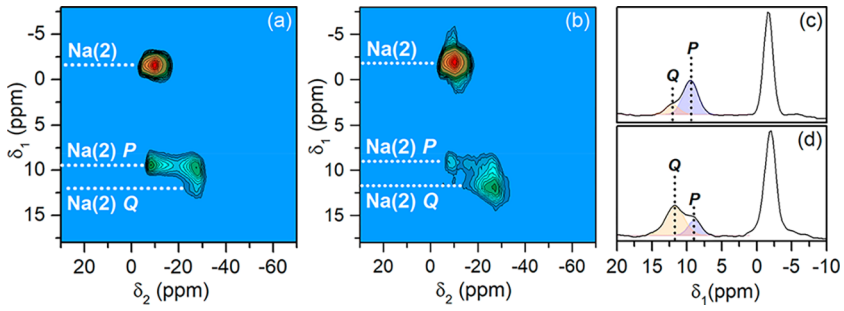

Figure 6. ^{23}Na STMAS spectra and projections along the indirect dimension for ceramic $NaNbO_3$: (a and c) with an average grain size of 1.07 μm where a fit using two Gaussian lines gives a relative content of ca. 20% *Q* phase (previous results stating <5%); (b and d) with an average grain size of 0.19 μm and ca. 75% *Q* phase (previous results stating 85%).

https://dx.doi.org/10.1021/acs.jpcc.0c07202
J. Phys. Chem. C 2020, 124, 23852−23858

reported from the STMAS spectra. These results can be taken as indicative that the method presented in this paper is more sensitive to small phase fractions, especially of the Q phase, and that the degree of phase coexistence might be underestimated when other NMR[11] or X-ray diffraction[10] methods are employed.

CONCLUSIONS

^{23}Na STMAS solid-state NMR experiments have been demonstrated to be a capable tool for the characterization of coexisting *P* and *Q* polymorphs in $NaNbO_3$. Phase quantification is more easily achieved by separation of the corresponding signals in the indirect dimension at lower magnetic field, and the insufficient signal-to-noise ratio in spectra recorded at low fields for relatively small pieces of ceramic samples can be compensated by switching from 3QMAS to STMAS. In a suitably low magnetic field, the quantification of *P* and *Q* polymorphs present in the sample can be easily done by integration across the indirect dimension of the spectrum with an estimated uncertainty of ±5%, which is similar to the analysis at high magnetic field. The STMAS pulse sequence opens a new venue for the exploration of AFE−FE phase coexistences in $NaNbO_3$-based lead-free antiferroelectrics. As the reliable quantification of coexisting, competing phases is a stepping stone toward a better understanding of these coexistences, further valuable insight into how antiferroelectric phases are stabilized and ferroelectric phases are minimized—and thus, how lead-free functional materials can be tailored for energy storage—can be expected.

ASSOCIATED CONTENT

Supporting Information

The Supporting Information is available free of charge at https://pubs.acs.org/doi/10.1021/acs.jpcc.0c07202.

^{23}Na STMAS spectrum of $NaNbO_3$ post electric field exposure, recorded at 14.1 T (Figure S1), STMAS/3QMAS comparison for commercial $NaNbO_3$ powder (Figure S2), and STMAS *P* and *Q* signal line shapes of ceramic $NaNbO_3$ with different grain sizes (Figure S3) (PDF)

AUTHOR INFORMATION

Corresponding Authors

Pedro B. Groszewicz − *Eduard Zintl Institute for Inorganic and Physical Chemistry and Department of Materials and Earth Sciences, Nonmetallic Inorganic Materials, Technical University of Darmstadt, 64289 Darmstadt, Germany; Department of Radiation Science and Technology, Delft University of Technology, Delft 2629JB, The Netherlands*; Email: p.groszewicz@tudelft.nl

Gerd Buntkowsky − *Eduard Zintl Institute for Inorganic and Physical Chemistry, Technical University of Darmstadt, 64289 Darmstadt, Germany*; orcid.org/0000-0003-1304-9762; Email: gerd.buntkowsky@chemie.tu-darmstadt.de

Authors

Sonja Egert − *Eduard Zintl Institute for Inorganic and Physical Chemistry, Technical University of Darmstadt, 64289 Darmstadt, Germany*

Mao-Hua Zhang − *Department of Materials and Earth Sciences, Nonmetallic Inorganic Materials, Technical University of Darmstadt, 64289 Darmstadt, Germany*; orcid.org/0000-0002-9823-4547

Jurij Koruza − *Department of Materials and Earth Sciences, Nonmetallic Inorganic Materials, Technical University of Darmstadt, 64289 Darmstadt, Germany*

Complete contact information is available at: https://pubs.acs.org/10.1021/acs.jpcc.0c07202

Notes

The authors declare no competing financial interest.

ACKNOWLEDGMENTS

This work was supported by the Hessian State Ministry for Higher Education, Research and the Arts under the LOEWE collaborative project "FLAME". Financial support by the Deutsche Forschungsgemeinschaft under Contract Bu-911-28-1 is gratefully acknowledged. P.B.G. gratefully acknowledges the Dutch Research Council (NWO) for the ECCM Tenure Track funding under Project Number ECCM.006.

REFERENCES

(1) Hao, X. A Review on the Dielectric Materials for High Energy-Storage Application. *J. Adv. Dielectr.* **2013**, *03*, 1330001.

(2) Liu, Z.; Lu, T.; Ye, J.; Wang, G.; Dong, X.; Withers, R.; Liu, Y. Antiferroelectrics for Energy Storage Applications: A Review. *Adv. Mater. Technol.* **2018**, *3*, 1800111.

(3) Shimizu, H.; Guo, H.; Reyes-Lillo, S. E.; Mizuno, Y.; Rabe, K. M.; Randall, C. A. Lead-Free Antiferroelectric: xCaZrO$_3$-(1-x)-NaNbO$_3$ System ($0 \leq x \leq 0.10$). *Dalton Trans.* **2015**, *44*, 10763−10772.

(4) Guo, H.; Shimizu, H.; Mizuno, Y.; Randall, C. A. Strategy for Stabilization of the Antiferroelectric Phase (*Pbma*) Over the Metastable Ferroelectric Phase ($P2_1ma$) to Establish Double Loop Hysteresis in Lead-Free (1−x)NaNbO$_3$-xSrZrO$_3$ Solid Solution. *J. Appl. Phys.* **2015**, *117*, 214103.

(5) Qi, H.; Zuo, R.; Xie, A.; Tian, A.; Fu, J.; Zhang, Y.; Zhang, S. Ultrahigh Energy-Storage Density in NaNbO$_3$-Based Lead-Free Relaxor Antiferroelectric Ceramics With Nanoscale Domains. *Adv. Funct. Mater.* **2019**, *29*, 1903877.

(6) Megaw, H. D. The Seven Phases of Sodium Niobate. *Ferroelectrics* **1974**, *7*, 87−89.

(7) Shuvaeva, V. A.; Antipin, M. Y.; Lindeman, R. S. V.; Fesenko, O. E.; Smotrakov, V. G.; Struchkov, Y. T. Crystal Structure of the Electric-Field-Induced Ferroelectric Phase of NaNbO$_3$. *Ferroelectrics* **1993**, *141*, 307−311.

(8) Cross, L. E.; Nicholson, B. J. The Optical and Electrical Properties of Single Crystals of Sodium Niobate. *Philos. Mag.* **1955**, *46*, 453−466.

(9) Wood, E. A.; Miller, R. C.; Remeika, J. P. The Field-Induced Ferroelectric Phase of Sodium Niobate. *Acta Crystallogr.* **1962**, *15*, 1273−1279.

(10) Zhang, M.-H.; Fulanović, L.; Egert, S.; Ding, H.; Groszewicz, P. B.; Kleebe, H.-J.; Molina-Luna, L.; Koruza, J. Electric-Field-Induced Antiferroelectric to Ferroelectric Phase Transition in Polycrystalline NaNbO$_3$. *Acta Mater.* **2020**, *200*, 127−135.

(11) Koruza, J.; Groszewicz, P.; Breitzke, H.; Buntkowsky, G.; Rojac, T.; Malič, B. Grain-Size-Induced Ferroelectricity in NaNbO$_3$. *Acta Mater.* **2017**, *126*, 77−85.

(12) Johnston, K. E.; Tang, C. C.; Parker, J. E.; Knight, K. S.; Lightfoot, P.; Ashbrook, S. E. The Polar Phase of NaNbO$_3$: A Combined Study by Powder Diffraction, Solid-State NMR, and First-Principles Calculations. *J. Am. Chem. Soc.* **2010**, *132*, 8732−8746.

(13) Zhelnova, O. A.; Fesenko, O. E. Phase Transitions and Twinning in NaNbO$_3$ Crystals. *Ferroelectrics* **1987**, *75*, 469−475.

(14) Ulinzheev, A. V.; Leiderman, A. V.; Smotrakov, V. G.; Topolov, V. Y.; Fesenko, O. E. Phase Transitions Induced in NaNbO$_3$ Crystals

by Varying the Direction of an External Electric Field. *Phys. Solid State* **1997**, *39*, 972−974.
(15) Li, W.; Xia, X.; Zeng, J.; Zheng, L.; Li, G. Significant Differences in $NaNbO_3$ Ceramics Fabricated Using Nb_2O_5 Precursors With Various Crystal Structures. *Ceram. Int.* **2020**, *46*, 3759−3766.
(16) Koruza, J.; Tellier, J.; Malič, B.; Bobnar, V.; Kosec, M. Phase Transitions of Sodium Niobate Powder and Ceramics, Prepared by Solid State Synthesis. *J. Appl. Phys.* **2010**, *108*, 113509.
(17) Ashbrook, S. E.; Le Pollès, L.; Gautier, R.; Pickard, C. J.; Walton, R. I. ^{23}Na Multiple-Quantum MAS NMR of the Perovskites $NaNbO_3$ and $NaTaO_3$. *Phys. Chem. Chem. Phys.* **2006**, *8*, 3423−3431.
(18) Eckert, H. Solid State NMR as a Tool of Structure and Dynamics in Solid State Chemistry and Materials Science: Recent Progress and Challenges. *Curr. Opin. Solid State Mater. Sci.* **1996**, *1*, 465−476.
(19) Züchner, L.; Chan, J. C. C.; Müller-Warmuth, W.; Eckert, H. Short-Range Order and Site Connectivities in Sodium Aluminoborate Glasses: I. Quantification of Local Environments by High-Resolution ^{11}B, ^{23}Na, and ^{27}Al Solid-State NMR. *J. Phys. Chem. B* **1998**, *102*, 4495−4506.
(20) Momma, K.; Izumi, F. *VESTA 3* for Three-Dimensional Visualization of Crystal, Volumetric and Morphology Data. *J. Appl. Crystallogr.* **2011**, *44*, 1272−1276.
(21) Ashbrook, S. E.; Wimperis, S. High-Resolution NMR of Quadrupolar Nuclei in Solids: The Satellite-Transition Magic Angle Spinning (STMAS) Experiment. *Prog. Nucl. Magn. Reson. Spectrosc.* **2004**, *45*, 53−108.
(22) Trebosc, J.; Amoureux, J.-P.; Gan, Z. Comparison of High-Resolution Solid-State NMR MQMAS and STMAS Methods for Half-Integer Quadrupolar Nuclei. *Solid State Nucl. Magn. Reson.* **2007**, *31*, 1−9.
(23) Pike, K. J.; Ashbrook, S. E.; Wimperis, S. Two-Dimensional Satellite-Transition MAS NMR of Quadrupolar Nuclei: Shifted Echoes, High-Spin Nuclei and Resolution. *Chem. Phys. Lett.* **2001**, *345*, 400−408.
(24) Amoureux, J.-P.; Pruski, M. MQMAS NMR: Experimental Strategies and Applications. *Encyclopedia of Magnetic Resonance* **2008**, 0319.
(25) Skibsted, J.; Nielsen, N. C.; Bildsøe, H.; Jakobsen, H. J. Satellite Transitions in MAS NMR Spectra of Quadrupolar Nuclei. *J. Magn. Reson.* **1991**, *95*, 88−117.
(26) Massiot, D.; Fayon, F.; Capron, M.; King, I.; Le Calvé, S.; Alonso, B.; Durand, J.-O.; Bujoli, B.; Gan, Z.; Hoatson, G. Modelling One- and Two-Dimensional Solid-State NMR Spectra. *Magn. Reson. Chem.* **2002**, *40*, 70−76.

https://dx.doi.org/10.1021/acs.jpcc.0c07202
J. Phys. Chem. C 2020, 124, 23852−23858